First-principles calculations on vibrational and dielectric properties of chalcopyrite $CuGaS_2$

2002 J. Phys.: Condens. Matter 14 7493

(http://iopscience.iop.org/0953-8984/14/32/309)

INSTITUTE OF PHYSICS PUBLISHING JOURNAL OF PHYSICS: CONDENSED MATTER

J. Phys.: Condens. Matter **14** (2002) 7493–7502 PII: S0953-8984(02)36175-7

First-principles calculations on vibrational and dielectric properties of chalcopyrite $CuGaS_2$

Mustafa Akdoğan and Resul Eryiğit[1]

Department of Physics, Abant Izzet Baysal University, Bolu-14280, Turkey

E-mail: resul@ibu.edu.tr

Received 24 April 2002, in final form 5 July 2002
Published 2 August 2002
Online at stacks.iop.org/JPhysCM/14/7493

Abstract

We have performed a first-principles study of structural, dynamical and dielectric properties of chalcopyrite semiconductor $CuGaS_2$. The calculations have been carried out within the local density functional approximation using norm-conserving pseudopotentials and a plane-wave basis. Born effective charge tensors, dielectric permittivity tensors, the phonon frequencies at the Brillouin zone centre and mode oscillator strengths are calculated using density functional perturbation theory. The calculated properties help resolve the source of some of the discrepancies in the experimental literature.

1. Introduction

The ternary I–III–VI_2 chalcopyrites form a large group of semiconductors with diverse structural, electrical and optical properties [1, 2]. One of this class of materials, $CuGaS_2$, is considered to be a promising material for nonlinear optical applications, partly because of its direct wide bandgap.

Over the last three decades the lattice dynamical properties of Cu-based chalcopyrites have been investigated experimentally as well as theoretically by a number of groups. Brillouin zone centre (BZC) phonon frequencies of $CuGaS_2$ have been measured by using Raman [3–8] and infrared (IR) [3, 9–11] spectroscopies. Earlier theoretical studies of chalcopyrite lattice dynamics were done by using phenomenological models, such as Born–von Karman [12], rigid ion [13], Urey–Bradley force field [14], valence force field [12], universal force field [15] and Keating models [16, 17]. Model calculations have two main drawbacks; the types of interaction they take into account might not be enough and their interaction parameters have to be derived from a fit to experimentally measured phonon frequencies. However, identification of lattice modes in experimental studies is sometimes incomplete, partly because of the complexity of the dispersion scheme in the chalcopyrite structure and partly because of experimental errors. Recently, first-principles calculations of lattice dynamics of chalcopyrite $AgGaSe_2$ [18–20], $AgGaTe_2$ [20], $AgGaS_2$ [21] and $CuInSe_2$ [22] have been reported. These calculations were

[1] Author to whom any correspondence should be addressed.

done by using a direct method where the phonon frequencies are calculated from Hellmann–Feynman forces generated by the small atomic displacements.

The first-principles investigation of phonon frequencies can be performed within a density functional perturbation theory (DFPT) [23], frozen-phonon [24] or direct method approach [19, 22]. The direct method is computationally straightforward and allows one to study both linear, such as phonons in the whole Brillouin zone, and nonlinear effects [22] with small computational effort. However, for polar crystals, there is a disadvantage of the direct method: the nonanalytic behaviour of dynamical matrices as functions of the wavevector in the long-wave limit, which causes the LO–TO splitting of zone centre optical modes, has to be supplied by a separate calculation using Berry's phase approach, borrowed from a DFPT calculation, fitted to experiment or obtained from use of an elongated supercell (for a review of DFPT and this issue, see [23]). In contrast to the direct method of calculating the phonon frequencies, the linear response approach lets one obtain the effective charges and dielectric tensors directly. To best of our knowledge, in all *ab initio* calculations of chalcopyrite phonon frequencies [18–22], the nonanalytic term is introduced from the experimental effective charges.

In this paper, we investigate the equilibrium lattice structure, Born effective charge tensors, dielectric permitivity tensors, zone centre phonon frequencies and mode oscillator strengths of $CuGaS_2$ using the density functional and DFPT [23, 25, 26]. Our aim is to help resolve the discrepancies in reported phonon frequencies and provide first-principles Born effective charges and dielectric tensors for direct method phonon calculations.

2. Method of calculation

The present results have been obtained thanks to the use of the ABINIT code[2], that is based on pseudopotentials and plane waves. It relies on an efficient fast Fourier transform algorithm [27] for the conversion of wavefunctions between real and reciprocal space, on the adaptation to a fixed potential of the band-by-band conjugate gradient method [28] and on a potential-based conjugate-gradient algorithm for the determination of the self-consistent potential [29].

The Troullier–Martins type pseudopotentials have been generated thanks to the FHI98PP code [30]. Special care has been used in constructing the pseudopotentials, in order to avoid the occurrence of ghost states [31] and to assure an optimal transferability over a wide energy range. The Cu pseudopotentials are obtained with parameters from [32]. We find that the inclusion of semicore states, such as 3d Cu, greatly improves the transferability of the pseudopotentials, and is at the same time necessary to take into account the hybridization of cation semicore states with anionic p states. The inclusion of Cu d states increases the kinetic energy cut-off of the plane waves included in the calculation because of the compact nature of these orbitals. The kinetic energy cut-off, E_{cut}, needed to obtain a convergence better than 0.01 eV of both total energy and Kohn–Sham eigenvalues is found to be equal to 40 Ha which is similar to convergence cut-offs of [32] (37.5 Ha) and [33] (35 Ha) that uses the same Cu pseudopotential. For linear response quantities reported in this paper, increasing E_{cut} from 35 to 40 Ha increases phonon frequencies by less than 2% and decreases effective charges and dielectric tensor components by less than 4%. The Brillouin zone is sampled by 12 special k points, which is found to be enough for convergence of static as well as response calculations.

Technical details on the computation of responses to atomic displacements and homogeneous electric fields can be found in [25], while [26] presents the subsequent computation of dynamical matrices, Born effective charges, dielectric permittivity tensors and interatomic force constants.

[2] The ABINIT code is a common project of the Universite Catholique de Louvain, Corning Incorporated and other contributors, URL http://www.abinit.org

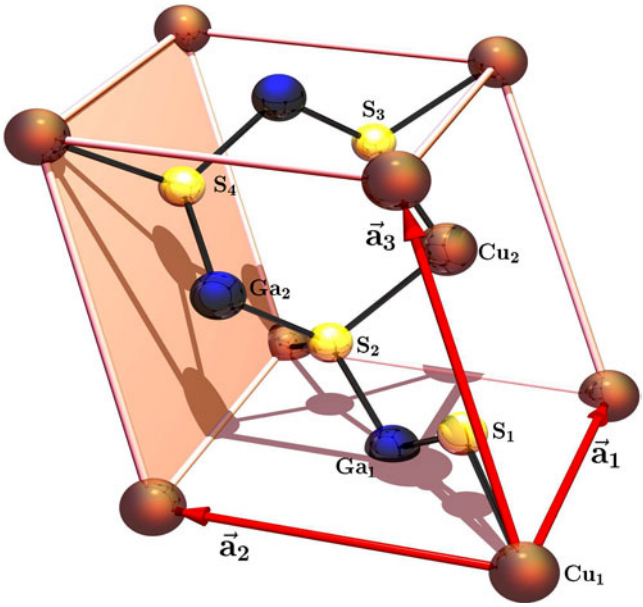

Figure 1. Primitive unit cell of chalcopyrite $CuGaS_2$.
(This figure is in colour only in the electronic version)

3. Results

3.1. Atomic structure

The chalcopyrite structure (space group D_{2d}^{12}, no 122) of I–III–VI_2 semiconductors can be considered as derived from the cubic zinc-blende structure (space group T_d^2) by populating one of the face-centred cubic sublattices with group VI atoms and the other one with equal numbers of group I and III atoms in a regular fashion. In general, I–VI and III–VI bond lengths, denoted by $d_{\mathrm{I-VI}}$ and $d_{\mathrm{III-VI}}$, respectively, are not equal. One consequence of having two different anion–cation bond lengths is a tetrahedral distortion characterized by $u = 0.25 + (d_{\mathrm{I-VI}}^2 - d_{\mathrm{III-VI}}^2)/a^2$ which describes the repositioning of the anions in the x–y plane; a is the lattice constant in the x or y direction. The second consequence of differing anion–cation bond lengths is a deformation of the unit cell along the z-direction to a length c which is generally different from $2a$. This tetragonal distortion is characterized by the quantity $\eta = c/a$.

The unit vectors of the primitive cell are $(a, 0, 0)$, $(0, a, 0)$, $(a/2, a/2, \eta a/2)$. The cations are located at 4a and 4b while anions are located at 8d Wyckoff positions. The primitive unit cell is displayed in figure 1.

The structural optimization was done by first determining the tetrahedral parameter u self-consistently by calculating the *ab initio* forces on the ions and, within the Born–Oppenheimer approximation, relaxing the position of each individual atom in the direction of the forces until the absolute values of the forces were converged to less than 0.01 mHa Bohr^{-1}. External parameters of the structure (a and c) are then determined by Broyden–Fletcher–Goldfarb–Shanno minimization (BFGS) of the energy.

The calculated lattice parameters, a, η and u, are compared to available experimental values in table 1. While the experimental values of a and η lattice parameters are measured with

Table 1. Calculated and experimental values of the cubic lattice constant a (in au), the tetragonal distortion parameter $\eta = c/a$ and tetrahedral distortion parameter u of the $CuGaS_2$ chalcopyrite structure.

	a	η	u
Calc.	10.36	1.954	0.267
Expt[a]	10.11	1.958	0.250
Expt[b]	10.12	1.948	0.275
Expt[c]	10.10	1.979	0.254

[a] Reference [34].
[b] Reference [35].
[c] Reference [36].

Table 2. Calculated Born effective charge tensors, $Z^\star$, eigenvalues of the symmetric part of $Z^\star(\lambda)$, average of eigenvalues ($\overline{\lambda}$) and experimental and BOM effective charges of [5].

Atom	$Z^\star$			λ	$\overline{\lambda}$	e_T^a	e_T^b
Cu_1	0.82	0.11	0.00	0.82	0.79	1.50	1.40
	−0.11	0.82	0.00	0.82			
	0.00	0.00	0.72	0.72			
Ga_1	2.61	0.10	0.00	2.82	2.68	1.60	2.00
	−0.10	2.61	0.00	2.61			
	0.00	0.00	2.82	2.61			
S_1	−1.53	0.00	0.00	−2.57	−1.73	−1.55	−1.70
	0.00	−1.89	0.70	−1.53			
	0.00	0.77	−1.78	−1.10			

[a] Dynamical charges from [5].
[b] Bond orbital charges from [5].

a high degree of accuracy, the u parameter is obtained in an indirect way and its reported values range from 0.250 to 0.275 for $CuGaS_2$ (see compilation by Jaffe and Zunger [37]). Considering the fact that the zero-point motion and thermal effects are not taken into account, the calculated lattice constant, tetragonal and tetrahedral distortion values agree with the experimental values quite well.

3.2. Born effective charge tensors

First, we present the Born effective charges, important ingredients of the present study since their knowledge allows us to identify the long-range part of the interatomic force constants and makes the interpolation of phonon frequencies tractable.

For insulators, the Born effective charge tensor for atom κ, $Z^\star_{\kappa,\beta\alpha}$, quantifies, to linear order, the polarization per unit cell, created along the direction β when the atoms of sublattice κ are displaced along the direction α, under the condition of zero electric field. It can be calculated from Berry phase or perturbation theory.

Our results for the dynamical effective charges of $CuGaS_2$ are presented in table 2 for three nonequivalent atoms. The effective charges for the other atoms can be obtained from those shown in the table by symmetry considerations. Because of finite k-point sampling there is a deviation from charge neutrality which is less than 0.01 electron for the unit cell. Because of tetragonal symmetry, effective charge tensor components of cations satisfy the relation $Z^\star_{xx} = Z^\star_{yy} \neq Z^\star_{zz}$. The anisotropy of $Z^\star_{\mathrm{Cu}}$ is opposite to and almost twice as large as that of $Z^\star_{\mathrm{Ga}}$. Because of the internal distortion, anions do not have equivalent effective charge tensors. The tetrahedral shifting of anion atoms creates four different configurations for these atoms

and the resulting effective charge tensor elements can be divided into two classes according to the magnitudes of $Z^{\star}_{xx}$ and $Z^{\star}_{yy}$. For all anions $Z^{\star}_{S,zz} = -1.78$ while $Z^{\star}_{S,xx}$ and $Z^{\star}_{S,yy}$ take the value -1.53 or -1.89 depending on the tetrahedral distortion of the x or y component of the position of the anion. Also, depending on the u distortion being along the x or y direction, the off-diagonal components $Z^{\star}_{S,zx}$, $Z^{\star}_{S,xz}$ or $Z^{\star}_{S,yz}$, $Z^{\star}_{S,zy}$ are different from zero.

Experimental effective charges of $CuGaS_2$ were investigated by Carlone *et al* [5]. They reported two sets of effective charges: one calculated from the measured BZC LO–TO splittings according to a modified Born model and one from the bond-orbital model (BOM) of Harrison [38]. In their computations, Born effective charges were assumed to be isotropic. Although it is not possible to compare our effective charge tensors with the scalar values reported in [5] directly, it is instructive to compare the averages of the eigenvalues of the symmetric part of the computed effective charge tensors. As can be seen from table 2, our average eigenvalues show a better agreement with BOM calculations of [5]; in particular the effective charge of sulfur calculated from BOM, -1.7, is very close to our calculated $\overline{\lambda_S} = -1.73$. The agreement for the effective charges of Cu and Ga is worse than that of S. This discrepancy is more pronounced for the effective charges calculated from the experimental LO–TO splittings and modified Born model, probably because of the use of approximate eigenvectors and assumptions about the dynamical charges. We have, also, calculated the effective charges of some other Cu-based chalcopyrite semiconductors ($CuInSe_2$ and $CuInS_2$ [39]) and found similar effective charges for these compounds.

The Born effective charge tensors of cations show very little anisotropy. If one assumes a Cu(+1)–Ga(+3)–S(-2) static ionic configuration for the $CuGaS_2$ compound, then the calculated Born effective charges are not very different from the static charges. The anomalous Born effective charge phenomenon, which is common for perovskites [40], is not seen for chalcopyrites.

3.3. Phonons

Since the primitive unit cell of the chalcopyrite structure has eight atoms, there are a total of 24 modes of vibration. A detailed discussion of group theoretical properties of chalcopyrite structure zone centre phonons can be found in [41]. The irreducible representation at the centre of the Brillouin zone is

$$\Gamma_{\text{opt}} = 1\Gamma_1 \oplus 2\Gamma_2 \oplus 3\Gamma_3 \oplus 3\Gamma_4 \oplus 6\Gamma_5$$

for optical modes, and

$$\Gamma_{\text{ac}} = 1\Gamma_4 \oplus 1\Gamma_5$$

for acoustic modes. Optical modes having Γ_1 and Γ_2 symmetry involve only displacement of anions. Γ_3, Γ_4 and Γ_5 symetry modes include displacement of cations, as well. Both Γ_4 and Γ_5 modes belong to vector transforming representations, and are thus IR active. Inclusion of the long range polarization interaction results in splitting of the Γ_4 and Γ_5 modes into TO and LO components, giving nine polar vibrations (three with polarization along c (Γ_4 modes) and six along x or $y(\Gamma_5)$). This results in different numbers of IR modes being active for $E \| c$ and $E \perp c$. Except modes of Γ_2 symmetry, all optical modes are Raman active.

In table 3 we display the typical eigendisplacement patterns of various modes of $CuGaS_2$. As can be seen from this table, the IR active Γ_4 mode involves in-phase motion of each cation pair and that of two anion pairs along the principal axis and as a result has a dipole moment in that direction. For the IR active Γ_5 mode, the resultant motion of each cation pair and that of each anion pair are along either the x or the y axis which causes twofold degeneracy and a dipole moment in the x–y plane. The Γ_1 and Γ_3 modes are out-of-phase motion of ions and

Table 3. Eigendisplacements for the zone centre optical modes of $CuGaS_2$. The upper signs (+ or −) correspond to the displacement patterns for one Cu, one Ga and two S ions while the lower signs to the displacement patterns for the remaining one Cu, one Ga and two S ions in the primitive cell. For the corresponding frequencies see table 4.

Mode	Cu_1	Ga_1	S_1	S_3
Γ_1	[0.00 0.00 0.00]	[0.00 0.00 0.00]	[∓2.07 0.00 0.00]	[0.00 ∓2.07 0.00]
Γ_2	[0.00 0.00 0.00]	[0.00 0.00 0.00]	[0.00 ∓1.12 1.74]	[±1.11 0.00 −1.74]
	[0.00 0.00 0.00]	[0.00 0.00 0.00]	[0.00 ±1.74 1.11]	[∓1.74 0.00 −1.11]
Γ_3	[0.00 0.00 ∓0.16]	[0.00 0.00 ±0.81]	[±1.88 0.00 0.00]	[0.00 ∓1.88 0.00]
	[0.00 0.00 ±0.83]	[0.00 0.00 ±1.68]	[∓0.72 0.00 0.00]	[0.00 ±0.72 0.00]
	[0.00 0.00 ∓1.90]	[0.00 0.00 ±0.66]	[∓0.47 0.00 0.00]	[0.00 ±0.47 0.00]
Γ_4	[0.00 0.00 −0.06]	[0.00 0.00 0.81]	[0.00 ±1.70 −0.82]	[±1.70 0.00 −0.82]
	[0.00 0.00 0.77]	[0.00 0.00 0.66]	[0.00 ∓1.03 −1.47]	[∓1.03 0.00 −1.47]
	[0.00 0.00 1.53]	[0.00 0.00 −1.21]	[0.00 ±0.58 −0.20]	[±0.58 0.00 −0.20]
Γ_5	[0.03 −0.02 0.00]	[0.70 0.38 0.00]	[0.01 −1.66 ±1.92]	[−0.03 0.85 ±0.03]
	[0.16 −0.10 0.00]	[0.43 −1.09 0.00]	[0.09 0.27 ∓0.66]	[0.01 2.23 ∓0.03]
	[0.27 −0.70 0.00]	[0.35 −0.17 0.00]	[0.03 0.72 ±0.70]	[−1.77 −0.01 ∓1.72]
	[0.73 −0.95 0.00]	[−1.36 0.52 0.00]	[0.07 −0.14 ±0.29]	[0.00 1.00 ±0.02]
	[0.25 −1.29 0.00]	[1.14 0.81 0.00]	[0.00 0.62 ∓0.72]	[0.04 −0.02 ∓0.05]
	[0.33 −1.84 0.00]	[−0.41 −0.32 0.00]	[−0.66 −0.05 ∓0.05]	[0.52 −0.06 ±0.60]

they do not have a dipole moment, so they are Raman active but not IR active. The Γ_2 mode is out-of-phase motion of anion pairs and does not produce a dipole moment.

In table 4 our calculated zone centre phonon frequencies and their symmetry assignments are displayed along with experimental data obtained by IR [3, 10, 11] and Raman [3, 5–8] measurements. We also present the root mean square relative deviation of our results with experimental data in the same table. For some of the modes there are large differences among the reported experimental frequencies, for example the highest frequency Γ_3 mode ranges from 7.28 [3] to 12.02 [5] THz. Our calculated value for this mode is close to 10.73 THz measured by [8] and [7]. Reported values of the other Γ_3 modes have similar discrepancies and we find the best agreement with data of [8] and [7]. The situation for IR active Γ_4 modes is somewhat different; except early Raman [3] and IR [11] studies, all reported frequencies show reasonable agreement. The problem with [3] and [11] seems to be a mistaken assignment for the second highest frequency Γ_4 mode. The experimental data for Γ_5 modes show a better consistency than other modes. Based on rms values in table 4, our calculated values show a better agreement with Raman data of Koschel [8] and Gonzalez [7] and IR data of Bodnar *et al* [10]. If we changed the symmetry assignments of some of the Γ_4 modes of [3] and [11], all sets would be in a similar agreement. It is reasonable to claim that most of the discrepancy in the reported zone centre phonon frequency data of $CuGaS_2$ is due to wrong symmetry assignments.

3.4. Lattice dielectric tensors

The calculated electronic (ϵ_∞) and static (ϵ_0) dielectric tensors are diagonal and have two independent components $\epsilon^{||}$ and $\epsilon^{\perp}$ along and perpendicular to the c axis, respectively. The electronic components are $\epsilon_\infty^{xx} = \epsilon_\infty^{yy} = 7.71$ and $\epsilon_\infty^{zz} = 7.54$ and static components are $\epsilon_0^{xx} = \epsilon_0^{yy} = 9.98$ and $\epsilon_0^{zz} = 10.23$. The static and high frequency dielectric tensors are almost isotropic, with an anisotropy of ≈2%, which is consistent with the fact that for $CuGaS_2$ tetragonal distortion is very small ($\eta \approx 2$).

Table 4. Zone centre phonon frequencies of $CuGaS_2$ (in THz).

Mode	Theory	Experimental results								
	This work	R [3]	R [4]	R [5]	R [6]	R [7]	R [8]	IR [10]	IR [3]	IR [11]
Γ_1	8.70	9.35	9.35	9.35	9.35	9.35	9.35			
Γ_2	10.25									
	8.06									
Γ_3	9.89	7.28		12.02		10.73	10.73			
	5.87	6.08	7.19	7.13	6.08	6.05	6.08			
	2.97	4.14	3.51	3.48	4.11	2.97	2.91			
Γ_4^{LO}	11.54	12.05	11.78	11.78	11.96	11.96	12.02	11.69	11.99	11.69
	7.52	11.06	8.33	8.63	8.39	8.33	8.42	8.39	7.44	10.37
	2.97	8.51	2.85	2.85	2.85	2.85	2.85			8.27
Γ_4^{TO}	10.63	11.12	10.97	11.00	10.94	11.03	11.03	10.85	11.08	10.85
	7.03	10.16	7.85	8.03	7.79	7.73	7.85	7.79	7.67	9.89
	2.96	7.76	2.85	2.85	2.85	2.85	2.85			7.67
Γ_5^{LO}	11.01	11.60	11.57	11.54	11.57	11.60	11.51	12.02	11.54	11.45
	9.83	10.55	10.55	10.40		10.43	10.55	10.49	10.49	10.49
	7.22	8.33	8.30	8.48	8.24	8.12	8.27	8.27	8.39	8.39
	4.87	5.00	4.98	5.00	5.51	4.95	4.80	4.80	5.49	
	3.50	2.94		4.41		3.48				
	2.50	2.28	2.25	2.25	2.22	2.22	2.22		2.01	
Γ_5^{TO}	10.37	10.94	10.94	11.00	10.94	10.91	10.88	10.97	10.97	10.97
	9.40	10.04	9.95	9.95	9.95	9.95	9.95	9.89	9.89	10.31
	7.08	7.79	7.79	8.18	7.79	7.73	7.85	7.67	7.49	7.49
	4.85	4.41	4.98	5.00	4.41	4.95	4.68	4.74	5.37	
	3.50	2.85		4.41		3.48				
	2.50	2.25	2.25	2.25	2.22	2.22	2.22		1.92	
		Rms relative deviations								
		0.25	0.08	0.11	0.09	0.07	0.07	0.05	0.10	0.21

We display our calculated dielectric tensor components along with model calculations of [42] and experimentally available values in table 5. The averages of ϵ_∞ and ϵ_0, obtained from the expression ϵ_∞ (or ϵ_0) $= (2\epsilon_\infty^\perp + \epsilon_\infty^\parallel)/3$ are also shown in this table. There are two problems with the comparison of our calculated values with experimental ones. The first problem is with the DFT–LDA approach: the theoretical calculation of dielectric constant within the DFT–LDA framework, in general, overestimates the experimental values [43–45]. The other problem is with the experimental data for high frequency and static dielectric constants of $CuGaS_2$, which show considerable differences. For example, $\epsilon_0^\parallel$ of [10] is 8.88 while the same quantity is reported to be 7.60 by Baars and Koschel [9]. In the course of investigating the dielectric properties of Cu-based chalcopyrite semiconductors [39], we have found that some of the similar discrepancies for experimental dielectric tensors of $CuInSe_2$ could be resolved by fitting the measured IR reflectivity with a different dielectric model from the one used in the reporting paper. Taking into account the fact that DFT–LDA overestimation is, generally, around 10% [40], static and electronic dielectric constants reported by [10] seem to be more consistent set than Bodnar's data [9].

The static dielectric tensor can be decomposed into the contributions of different modes as follows [25]:

Table 5. Static and high frequency dielectric tensor components of $CuGaS_2$.

	$\epsilon_\infty^\parallel$	$\epsilon_\infty^\perp$	ϵ_∞	$\epsilon_0^\parallel$	$\epsilon_0^\perp$	ϵ_0
Calc.	7.54	7.71	7.66	10.23	9.98	10.06
Model[a]	5.50	5.60	5.57	7.60	7.80	7.73
Expt[b]	6.10	6.20	6.17	7.60	8.90	8.47
Expt[c]	5.89	6.27	6.14	8.88	8.25	8.46

[a] Reference [42].
[b] Reference [9].
[c] Reference [10].

$$\epsilon_{\alpha\beta}^0 = \epsilon_{\alpha\beta}^\infty + \frac{4\pi}{\Omega_0}\sum_m \frac{S_{m,\alpha\beta}}{\omega_m^2} \tag{1}$$

where Ω_0 is the volume of the primitive unit cell, ω_m is the frequency of mode m and $S_{m,\alpha\beta}$ is the oscillator strength tensor which is related to eigendisplacements $U_m(\kappa\alpha)$ and Born effective charge tensors by

$$S_{m,\alpha\beta} = \left(\sum_{\kappa\alpha'} Z^\star_{\kappa,\alpha\alpha'} U^\star_m(\kappa\alpha')\right)\left(\sum_{\kappa'\beta'} Z^\star_{\kappa',\beta\beta'} U^\star_m(\kappa'\beta')\right). \tag{2}$$

Similarly, one can define a mode-effective charge tensor as

$$Z^\star_{m,\alpha} = \frac{\sum_{\kappa\beta} Z^\star_{\kappa,\alpha\beta} U_m(\kappa\beta)}{[\sum_{\kappa\beta} U^\star_m(\kappa\beta) U_m(\kappa\beta)]^{1/2}}. \tag{3}$$

For IR active modes the relevant components of the oscillator strength tensor (zz component for Γ_4 and xx component for Γ_5 modes) and the magnitude of mode effective charge tensor along with experimental oscillator strength data from [10] are displayed in table 6. Both Γ_4 and Γ_5 symmetry higher frequency modes have higher mode effective charges and oscillator strengths. For Γ_5 modes, except for the second highest frequency mode, the agreement between calculated and experimental oscillator strengths is satisfactory. However, for Γ_4 modes the agreement with [10] and [9] is only qualitative; the lowest frequency mode has a much smaller S_m compared to other Γ_4 modes and the highest frequency mode has the largest S_m. Since the mode contribution to the static dielectric constant is inversely proportional to the square of the mode frequency (equation (1)), low frequency modes of both Γ_4 and Γ_5 symmetry contribute to ϵ_0 considerably, although their oscillator strengths are smaller compared to higher frequency modes.

4. Conclusion

We have investigated the dynamical properties, such as Born effective charge tensor, BZC phonon frequencies and static and high frequency dielectric tensors of the ternary semiconductor $CuGaS_2$ within the DFPT. From a comparison of our first-principles results with several sets of experimental data for zone centre phonon frequencies of $CuGaS_2$, one can claim that some of the symmetry assignments of reported zone centre Γ_3 and Γ_4 modes should be changed. Also, our calculated static and high frequency dielectric tensors help resolve the discrepancies in the reported experimental data. We have also computed mode oscillator strengths and mode effective charges of the IR active modes and found fair agreement with the experiments.

Table 6. The relevant oscillator strength tensor components S_m (in 10^{-4} m^3 s^{-2}), magnitude of mode-effective charge vectors $Z^{\star}_m$ and LO frequencies ω_m (in THz) of IR active modes of $CuGaS_2$.

	S_m				
	Calc.	Expt[a]	Expt[b]	$Z^{\star}_m$	ω_m
Γ_4	1.64			0.81	2.97
Γ_4	16.87	8.38	4.25	3.27	7.52
Γ_4	23.57	16.26	15.72	4.40	11.54
Γ_5	0.52			0.00	2.50
Γ_5	1.52			0.10	3.50
Γ_5	2.74	2.74	0.68	0.41	4.87
Γ_5	9.44	8.14	8.78	1.85	7.22
Γ_5	20.34	13.10	7.20	3.95	9.83
Γ_5	15.48	17.19	12.82	2.85	11.01

[a] Reference [10].
[b] Reference [9].

Acknowledgment

We thank Bilkent University High Performance Computing Centre for allocation of computing time on their machines.

References

[1] Gaber A M, Tuttle J R, Albin D S, Tennant A L and Contreras M A 1994 *12th NREL Photovoltaic Program Review (AIP Conf. Proc. vol 306)* ed R Noufi p 59
[2] Birkmire R W and Eser E 1997 *Annu. Rev. Mater. Sci.* **27** 625
[3] van der Ziel J P, Meixner A E, Kasper H M and Ditzenberger J A 1974 *Phys. Rev.* B **9** 4286
[4] Bodnar I V, Smirnova G F, Karoza A G and Chernyakova A P 1990 *Phys. Status Solidi* b **158** 469
[5] Carlone C, Olego D, Jayaraman A and Cardona M 1980 *Phys. Rev.* B **22** 3877
[6] Anedda A, Bongiovanni G and Raga F 1983 *Nuovo Cimento* **2** 1950
[7] Gonzalez J and Fernandez B J 1992 *Phys. Rev.* B **46** 15 092
[8] Koschel W H and Bettini M 1972 *Phys. Status Solidi* b **72** 729
[9] Baars J and Koschel W H 1972 *Solid State Commun.* **11** 1513
[10] Bodnar I V 1998 *Semiconductors* **32** 613
[11] Bodnar I V, Karoza A G and Smirnova G F 1977 *Phys. Status Solidi* b **84** K65
[12] Fouret R, Derollez P, Laamyem A, Hennion B and Gonzalez J 1997 *J. Phys.: Condens. Matter* **9** 6579
[13] Ohrendorf F W and Haeuseler H 1999 *Cryst. Res. Technol.* **34** 339
[14] Lauwers H A and Herman M A 1977 *J. Phys. Chem.* **38** 983
[15] Lazewski J and Parlinski K 2000 *Phys. Status Solidi* b **218** 411
[16] Bettini M 1975 *Phys. Status Solidi* b **69** 201
[17] Artus L, Pujol J, Pascual J and Camassel J 1990 *Phys. Rev.* B **41** 5727
[18] Karki B B, Clark S J, Warren M C, Hsueh H C, Ackland G J and Crain J 1997 *J. Phys.: Condens. Matter* **9** 375
[19] Ackland G J, Warren M C and Clark J S 1997 *J. Phys.: Condens. Matter* **9** 7861
[20] Lazewski J and Parlinski K 1999 *J. Phys.: Condens. Matter* **11** 9673
[21] Lazewski J and Parlinski K 2001 *J. Chem. Phys.* **114** 6734
[22] Lazewski J, Parlinski K, Hennion B and Fouret R 1999 *J. Phys.: Condens. Matter* **11** 9665
[23] Baroni S, de Gironcoli S, dal Corso A and Giannozzi P 2001 *Rev. Mod. Phys.* **73** 515
[24] Kunc K and Martin R M 1983 *Ab Initio Calculation of Phonon Spectra* ed J T Devreese, V E van Doren and P E van Camp (New York: Plenum) p 63
[25] Gonze X 1997 *Phys. Rev.* B **55** 10 337
[26] Gonze X and Lee C 1997 *Phys. Rev.* B **55** 10 355
[27] Goedecker S 1997 *SIAM J. Sci. Comput.* **18** 1605
[28] Payne M C, Teter M P, Allan D C, Arias T A and Joannopoulos J D 1992 *Rev. Mod. Phys.* **64** 1045

[29] Gonze X 1996 *Phys. Rev.* B **54** 4383
[30] Fuchs M and Scheffler M 1999 *Comput. Phys. Commun.* **119** 67
[31] Gonze X, Stumpf R and Scheffler M 1991 *Phys. Rev.* B **44** 8503
[32] Fuchs M, Bockstedte M, Pehlke E and Scheffler M 1998 *Phys. Rev.* B **57** 2134
[33] Roundy D, Krenn C R, Cohen M L and Morris J W 1999 *Phys. Rev. Lett.* **82** 2713
[34] Hahn H, Frank G, Klingler W and Storger G 1983 *Z. Anorg. Chem.* **271** 153
[35] Spies H W, Haeberln V, Brandt G, Rauber A and Schneider J 1974 *Phys. Status Solidi* b **62** 183
[36] Abrahams S C and Bernstein J L 1973 *J. Chem. Phys.* **59** 5415
[37] Jaffe J E and Zunger A 1984 *Phys. Rev.* B **29** 1882
[38] Harrison W 1980 *Electronic Structure and the Properties of Solids* (San Francisco, CA: Freeman) p 222
[39] Parlak C and Eryiğit R 2002 to be published
[40] Ghosez Ph, Michenaud J P and Gonze X 1998 *Phys. Rev.* B **58** 6224
[41] Tanino H, Maeda T, Fujikake H, Nakanishi H, Endo S and Irie T 1992 *Phys. Rev.* B **45** 13 323
[42] Marquez R and Rincon C 1995 *Phys. Status Solidi* b **191** 115
[43] Gonze X, Ghosez Ph and Godby R W 1995 *Phys. Rev. Lett.* **74** 4035
[44] Martin R M and Ortiz G 1997 *Phys. Rev.* B **56** 1124
[45] Ghosez Ph, Gonze X and Godby R W 1997 *Phys. Rev.* B **56** 12 811